Assessment of the non-linear behaviour of plastic ankle foot orthoses by the finite element method

S Syngellakis[1]*, **M A Arnold**[1] and **H Rassoulian**[2]
[1]School of Engineering Sciences, University of Southampton, UK
[2]Department of Medical Physics and Bioengineering, Southampton General Hospital, UK

Abstract: The stiffness characteristics of plastic ankle foot orthoses (AFOs) are studied through finite element modelling and stress analysis. Particular attention is given to the modelling and prediction of non-linear AFO behaviour, which has been frequently observed in previous experimental studies but not fully addressed analytically. Both large deformation effects and material non-linearity are included in the formulation and their individual influence on results assessed. The finite element program is subsequently applied to the simulation of a series of tests designed to investigate the relation between AFO trimline location and stiffness for moderate and large rotations. Through careful consideration and identification of key modelling parameters, the developed finite element solution proves to be a reliable and effective alternative means of assessing variations of a typical plastic AFO design so that particular patient requirements could be met, in the long term.

Keywords: ankle foot orthosis, orthosis stiffness, orthosis trimline, plantar flexion, dorsiflexion, polypropylene, non-linearity, finite elements

NOTATION

E	Young's modulus
F	nodal reaction
FL	foot length
LL	leg length
LMH	lateral malleolus height
LW	leg width
M	ankle moment
R	distance from the ankle joint to a node in the distal foot region
R'	distance from the ankle joint to a node in the posterior foot region
δ_x, δ_y	nodal displacements in the sagittal plane
δ_z	maximum medio-lateral displacement
δ_m	maximum foot displacement
θ_f	foot rotation angle about the ankle joint axis
σ_e	von Mises stress

Abbreviation

MPJ	metatarsophalangeal joint

The MS was received on 8 July 1999 and was accepted after revision for publication on 5 October 1999.
** Corresponding author: School of Engineering Sciences, University of Southampton, Highfield, Southampton SO17 1BJ, UK.*

1 INTRODUCTION

An ankle foot orthosis (AFO) is a device widely prescribed to patients with various lower limb muscle and joint weaknesses and instabilities [**1**]. The plantar flexion and dorsiflexion resistance requirements of an AFO range widely depending on the patient's condition. Therefore, a customized AFO design can be achieved only if its stiffness can be predicted with a certain degree of confidence. Polypropylene AFOs have definitive, well-documented advantages over the conventional designs with metal uprights [**1**] but their mechanical behaviour under service conditions cannot be easily predicted [**2**]. This restricts the ability to match a plastic AFO to the needs of a particular patient. For this reason, considerable research effort has been focused over the last 20 years or so on the experimental measurement of the key stiffness characteristics of common AFO designs [**2–10**].

The use of computers facilitates the customized design of the AFO to support the uniquely shaped lower limb with the obvious advantages of flexibility of design, speed of production, consistency of quality and standardization [**11**]. Such computer-aided bioengineering can be combined with analytical simulation, which, compared with experimentation, offers the advantage of versatility in the choice of geometry and material but requires the validity of its predictions to be confidently

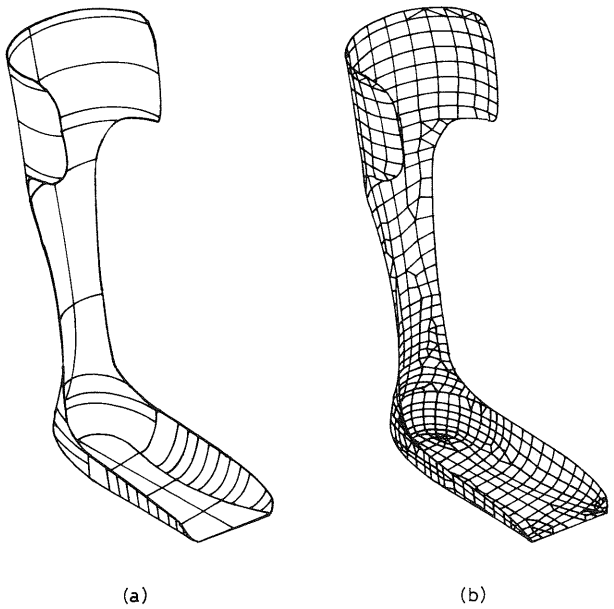

Fig. 1 An example of (a) a prefabricated AFO and (b) its finite element mesh

established. The problem considered in this paper is illustrated in Fig. 1: a prefabricated AFO intended for patients suffering from drop-foot is drawn in Fig. 1a, a possible finite element model of the AFO is shown in Fig. 1b.

Several numerical analyses of plastic AFOs, based on the finite element method (FEM), have been attempted [**12–16**]. In most of the analyses the behaviour of the device was assumed to be linear, i.e. large deformation and material non-linearity effects were ignored. However, since the rotations of the foot region of the AFO about the ankle joint axis can become quite large, the original stiffness matrix, calculated using the coordinates of the undeformed configuration, does not accurately represent the stiffness of the deformed device. It is also known that polypropylene is a non-linear material beyond a certain loading range. Clear evidence of the geometrically and materially non-linear behaviour of AFOs has been produced from several test programmes [**2, 4–6**].

The only known previous non-linear FEM analysis was performed on a three-dimensional model consisting of thick shell elements [**15**]. This allowed the behaviour of an AFO during dorsiflexion to be investigated by predicting instability loads and comparing them with those obtained from tests. Initially, a linear analysis yielded the Euler buckling load, which is an upper limit to the actual buckling load. In order to simulate the large deflections observed in tests, a geometrically non-linear analysis was then performed, involving incremental loading and an iterative solution technique. The resulting load versus deflection plot followed a similar trend to that of the test results, i.e. the curve became non-linear after a certain point showing decreasing stiffness, although the magnitude of the theoretical loading was substantially greater than that of the experimental loading for a set deflection. It was suggested that refinements in the model, including the use of non-linear material properties and modelling the entire AFO geometry, could bring the analytical results in line with the experimental data, although at a cost of increased processing time.

There was therefore considerable scope for the development of a more general and properly validated large deformation AFO analysis, which would yield reliably accurate flexibility results. The work described in this paper includes a versatile computer graphics procedure for generating an AFO solid model and the experimental assessment of material non-linearity under static loading. Initially, the FEM analysis is applied to a typical, arbitrarily defined AFO design in order to assess independently the effect of geometric and material non-linearity. This is followed by a systematic simulation of a series of experiments with AFO specimens of variable flexibility in order to establish the effectiveness, efficiency and validity of the method in predicting real AFO behaviour.

2 FINITE ELEMENT MODEL

2.1 Geometric model

The generation of the geometric model of a leg was the first step towards building the finite element model of an AFO fitting that leg. For this purpose, the coordinates of several points located on the surface of a normal human right lower limb were measured from drawings of lateral and anterior profiles of the limb as well as the transverse profile of the foot. These points were distributed around the circumference of a number of cross-sections through the leg/foot. A computer model of the limb was then developed using the pre-processor of the general purpose, finite element analysis (FEA), software ANSYS, version 5.1 [**17**]. The identified points at each individual cross-section were connected by splines to form near-closed lines encircling the limb. The result was a wire frame approximating the geometry of the leg. Finally, the surface area of the leg was constructed as a single, continuous area by 'skinning' a surface through these contour lines.

The AFO was then cut out of this leg shell by defining a surface of cut and performing a Boolean subtraction. The surface of cut was identified in two stages. First, the trimline was defined relative to the two-dimensional projection of the leg on the sagittal plane as shown in Fig. 2. A set of parameters were selected defining the position of the main points 'A' to 'J' and the radii of arcs centred at points E and H. These parameters permit quantification of a trimline used prospectively within a CAD/FEA environment. The adopted values for the

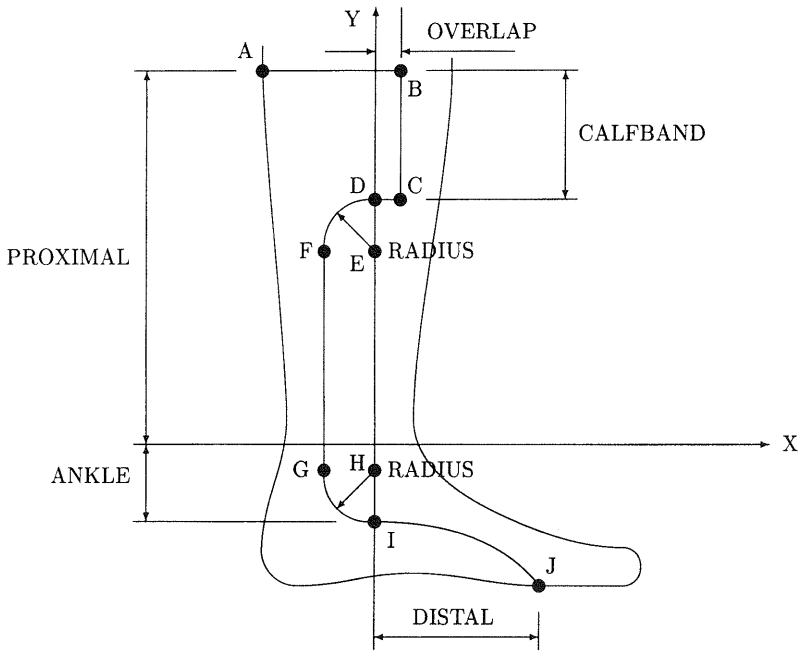

Fig. 2 A two-dimensional view of the trimline with the parameters defining its geometry

trimline parameters in the sensitivity studies (proximal = 260 mm, distal = 110 mm, calfband = 80 mm, overlap = ankle = radius = 30 mm) were selected arbitrarily but ensuring that the final geometry of the AFO looked as realistic as possible. An alternative trimline profile, duplicating that of an actual AFO specimen, was drawn for the validation analyses.

The two-dimensional trimline was then dragged parallel to the Z axis to form a continuous cylindrical surface, effectively projecting it on to the leg's shell in the Z direction as shown in Fig. 3. The subsequent Boolean subtraction transferred the trimline on to the shell as the line of cut. Because of the asymmetrical geometry of the leg, the medial and lateral parts of the obtained trimline turned out to be different. This is consistent with real AFO geometry since the orthotist usually adopts different trimline contours on either side. The model was divided into smaller areas of simple shape representing the medial and lateral regions of the foot, heel, calf and calfband. This facilitated mesh control, variable thickness definition and the application of loads and constraints to specific regions.

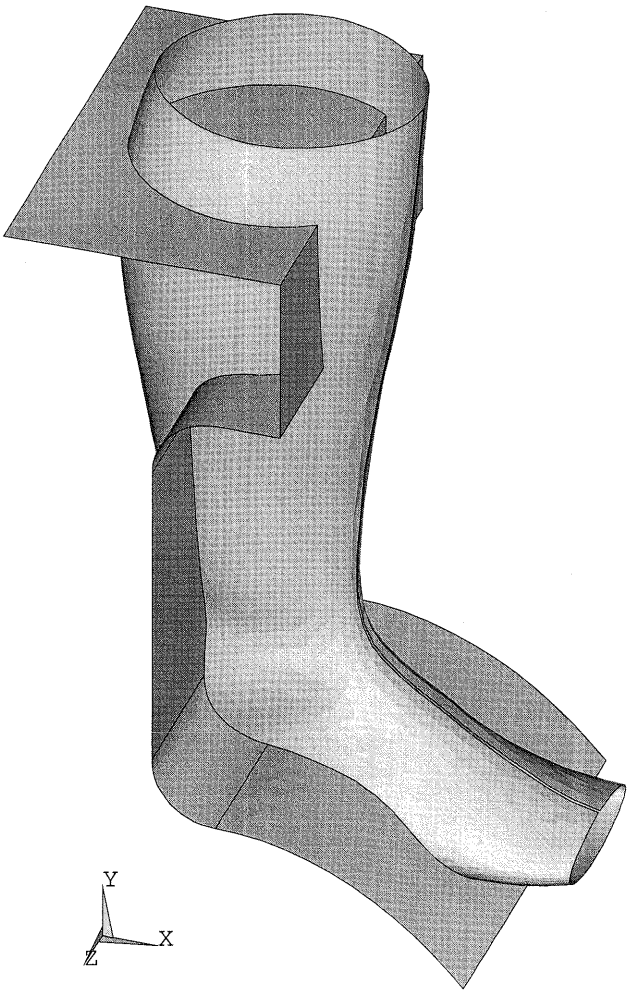

Fig. 3 Projecting the two-dimensional trimline on to the shell of the three-dimensional leg

2.2 Meshing

Because of the relative thinness of the AFO compared with its other dimensions and the curvature of its surface, the eight-node quadratic shell element available within ANSYS was thought to be the most appropriate element type. Since this shell element can fit a curved surface and have variable thickness, a sufficiently refined mesh of such elements can represent the three-dimensional geometry of the AFO quite accurately. It also has six

degrees of freedom (three translations and three rotations) per node; it can therefore be deformed and translated in any mode and direction in three-dimensional space.

The finite element model of the AFO was generated by automatic meshing of the solid model. This allowed direct mesh refinement based on energy error distributions for a series of linear static analyses [**18**]. Satisfactory convergence of both displacement and stress results was found with a mesh consisting of 1708 nodes and 549 elements. It was initially assumed that the analysed AFO had a constant thickness of 2 mm throughout.

2.3 Material

The glass transition temperature, the temperature at which a polymer changes from a rubbery to a glassy state upon cooling, has been reported as $-20\,^{\circ}C$ for polypropylene [**19**]. Above this temperature and hence at the operating temperature of an AFO, the relationship between stress and strain is non-linear [**20**]. A simple uni-axial tensile test was performed on a copolymer polypropylene specimen at a constant strain rate and temperature. The resulting stress–strain graph shown in Fig. 4 is non-linear with decreasing stiffness as the load increases. Since this result agreed with data presented by Ogorkiewicz [**21**], it was deemed sufficiently representative of the non-linear features of the material for the purposes of the developed analysis.

An appropriate model of material non-linearity had to be adopted. Since the non-linear deformation of polypropylene is mostly recoverable and the applied loading static and monotonic, the stress–strain relationship of Fig. 4 was modelled as multilinear elasticity. In this case, data for eight points were obtained from the experimental graph. The Young's modulus, E, at low stress was calculated from the initial slope and rounded up to the nearest integer of 1390 MPa, which is considerably higher than the constant value of 1000 MPa quoted in the technical literature [**22**]. Presumably, this lower value has been adopted for use in linear analyses to account, in a very approximate way, for the drop in stiffness at relatively low stress levels. The secant to the stress–strain curve of Fig. 4, corresponding to $E = 1000$ MPa, shows that a linear analysis with this reduced Young's modulus predicts the same strain as that measured at stresses in the region of 13 MPa.

Most plastics have a Poisson's ratio of between 0.35 and 0.45, and as the exact value is not critical, the value of 0.35 was adopted. Indeed, the response of the model was found to be nearly insensitive to changes in this material constant. Only isotropic properties were considered, although the elasticity of the material would actually be orthotropic as orientation is induced during the manufacture of the material sheet in the direction of draw [**23**]. The viscoelasticity of the material must also be accounted for if the AFO is to be subjected to repeated cyclic loading.

3 SENSITIVITY STUDIES

3.1 Constraints and loading

Partial constraints were applied to all the nodes of the two posterior areas in the proximal calf region to simulate the radial constraint provided due to the calf strap. This was achieved by adopting a nodal coordinate system for each of these nodes such that their nodal x axis intersected the vertical global Y axis. The con-

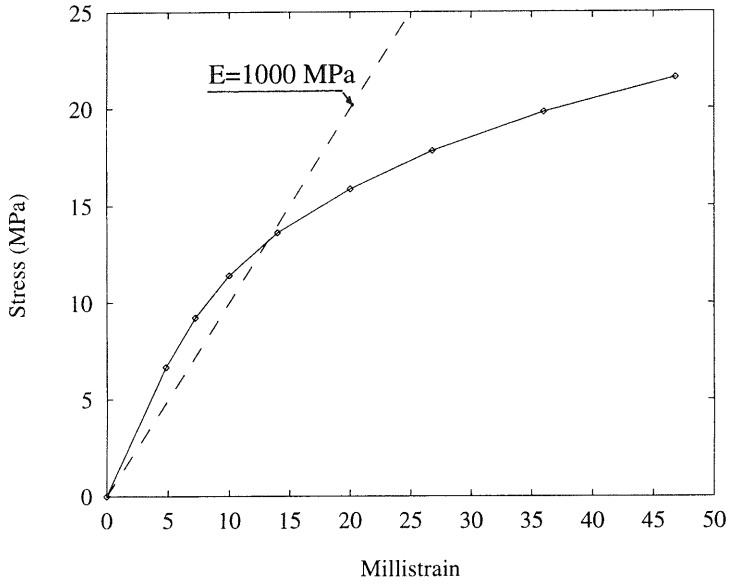

Fig. 4 Uni-axial stress–strain curve for polypropylene

straints were then applied at these nodes in the nodal x directions, while the remaining degrees of freedom were left free. The AFO was therefore free to move up and down the calf, or undergo internal and external rotations. Constraints were also applied to all nodes in the heel region to simulate the constraint provided by the shoe and foot. The nodal coordinate system at each of these nodes was first rotated such that its x axis passed through the global origin. Each node was then constrained in this direction, coincident to the radial direction of a spherical coordinate system, while remaining free to displace in all other directions. The constrained areas in the calf and heel regions as well as the orientation of nodal constraint are shown in Fig. 5.

In order to avoid artificial stress concentrations due to point loading and represent the rather smooth interaction expected between AFO and foot, the analyses were performed with a pressure of 8.65 kPa uniformly distributed over the distal part of the foot region as shown in Fig. 5. The predicted ankle rotations due to that pressure were close to the mean values, over a gait cycle, of recorded data for a number of orthoses [**3**]. The originally specified constraints at the foot/heel region were found to provide insufficient resistance against a rigid body rotation of the AFO caused by the off-centre resultant of the pressure acting on the asymmetric foot region. Therefore, an additional constraint was imposed in the global Z direction at a single node in the heel to eliminate this. It is worth noting that the possibility of AFO medio-lateral motion when loaded in the sagittal plane has been demonstrated experimentally [**10**].

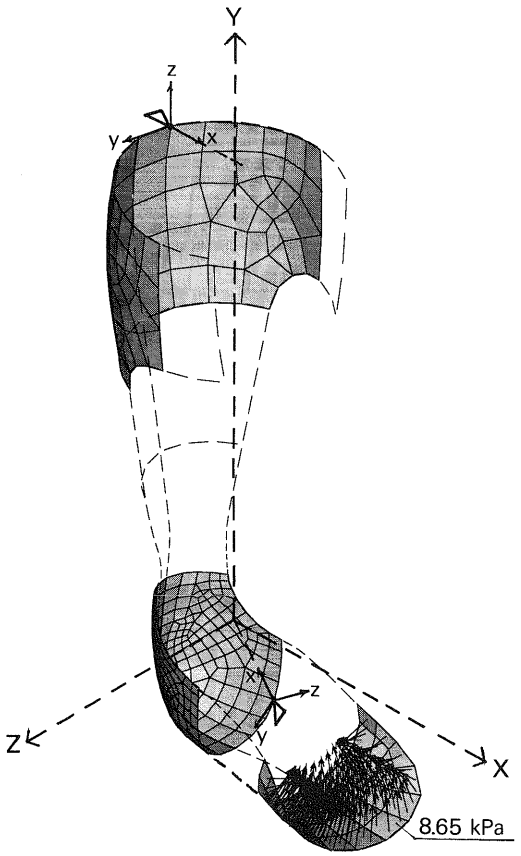

Fig. 5 Constraints and loading applied to the AFO model for the sensitivity studies

3.2 Geometric non-linearity

Only large deformation effects were activated first to investigate their significance. All non-linear problems are solved within ANSYS as a series of linear approximations using a Newton–Raphson iterative procedure. The program gave identical results with evenly spaced and automatic load stepping. Stress stiffening was also activated but was found to increase the number of equilibrium iterations without affecting the results. Analyses were performed for both plantar flexion and dorsiflexion motion, with a constant Young's modulus of 1000 MPa. The key results are listed in Table 1, along with results obtained from the linear analysis using the same mesh and loading conditions for comparison purposes.

It can be seen that, in plantar flexion, the non-linear predictions of maximum foot displacement δ_m, medial–lateral displacement δ_z and ankle rotation θ_f are greater by 13, 20 and 11 per cent, respectively, than the corresponding linear results for the same load. This difference is the consequence of accounting for the change of stiffness due to geometric changes during deformation. Surprisingly, AFO stiffness in dorsiflexion appears to be greater than that in plantar flexion, a result contradicting experimental evidence [**2**, **4**, **5**, **8**]. This was due to overconstraining the heel region in such a way as to inhibit the tendency of the AFO to expand along a medio-lateral line through the malleoli (see Fig. 5). More realistic heel constraints were introduced later in the context of a validation analysis. Nevertheless, it was shown at this stage that large deformation effects on the results are significant; different AFO behaviour in plantar flexion and dorsiflexion was also predicted. Due to the asymmetry of the model with respect to the sagittal plane, the foot region was predicted to deflect medially under plantar flexion and laterally under dorsiflexion. The linear and non-linear results for the medial–lateral displacement, δ_z, of the distal foot trimline are included in Table 1.

3.3 Material non-linearity

Two more analyses were performed with the non-linear elasticity of Fig. 4 but with the large deformation option disabled so that the effects of material non-linearity could be examined in isolation. The main results for both plantar flexion and dorsiflexion motion are listed in Table 2, along with the results from the linear analysis obtained for a Young's modulus of 1390 MPa, i.e. the initial slope of the non-linear stress–strain curve. The

Table 1 Results from analyses with linear, elastic material model ($E = 1000$ MPa)

Analysis type	Direction of ankle rotation	Maximum displacement δ_m (mm)	Maximum medial–lateral displacement δ_z (mm)	Rotation angle θ_f (degrees)	Maximum von Mises stress σ_e (MPa)
No large deformations	Either	10.2	−4.4	3.8	25.7
With large deformations	Plantar flexion	11.5	−5.3	4.2	28
	Dorsiflexion	8.9	2.7	3.5	22.4

Table 2 Results from analyses with non-linear, elastic material model

Analysis type	Direction of ankle rotation	Maximum deflection δ_m (mm)	Maximum medial–lateral displacement δ_z (mm)	Rotation angle θ_f (degrees)	Maximum von Mises stress σ_e (MPa)
Linear ($E = 1390$ MPa)	Either	7.3	−3.2	2.7	25.7
Non-linear (no large deformations)	Plantar flexion	7.5	−3.3	2.8	15.8
	Dorsiflexion	7.5	3.3	2.8	15.8
Non-linear (with large deformations)	Plantar flexion	8.3	−3.9	3.0	16.2
	Dorsiflexion	6.7	2.3	2.6	15.1

non-linear deformation results for both plantar flexion and dorsiflexion were very close to the corresponding linear predictions, probably due to the rather low load and the concentration of high stresses in small areas. Only the maximum von Mises stresses were found to be significantly lower than values obtained from the linear analysis, since the new material model imposes upper bounds to maximum stresses which are effectively forced to be redistributed over larger areas.

3.4 Combined non-linearities

The combined effect of both large deformation and multilinear elasticity was examined next by again subjecting the AFO to both plantar flexion and dorsiflexion motion. The results given in Table 2 reflect the individual characteristics of the two types of non-linearity discussed earlier. Again the model appears to be stiffer in dorsiflexion than in plantar flexion due to excessive constraint at the heel. Plots of maximum displacement versus pressure revealed that the AFO behaviour was only slightly non-linear as the load was increased, which did not seem unreasonable for the initial range of applied pressure. As the magnitude of the pressure was increased further, the non-linear behaviour of the AFO became more pronounced while the number of iterations per step increased.

It is interesting to compare the non-linear results of Table 2 with the respective linear ones in the first row of Table 1, obtained with a reduced Young's modulus of 1000 MPa. In the latter case, the assumed uniform reduction in material stiffness results in a more compliant AFO model than that predicted using geometric and material non-linearity which reduces stiffness only locally, i.e. at regions of high rotations and stress concentrations. This comparison confirms the view that a linear analysis with a constant Young's modulus leads to unreliable estimates of AFO stiffness.

3.5 Variable thickness

The thickness of a custom-made AFO, measured at a number of key locations, was found to vary significantly, particularly over the foot region. The minimum thickness, located at the heel region, was 54 per cent of the maximum thickness located at the posterior calf region. The average thickness around the ankle trimline was found to be approximately equal to 80 per cent of the maximum, which agreed with similar measurements by other investigators [**4**]. Due to the large size of the model, it would have been impractical to assign a different thickness at each individual node. For this reason, the AFO model was idealized as consisting of regions of constant thickness corresponding to the areas into which the geometric model had already been divided. Thickness values were assigned to the various areas such that their ratios to the maximum thickness of 2 mm were the same as the respective ratios in the custom-made AFO, evaluated using its average thickness over the corresponding regions.

The results of non-linear analyses with uniform and variable thickness are given in Table 3. The difference between predictions of deformation quantities in the two cases varies from 7 to 10 per cent. This indicates that

Table 3 Effect of thickness variation

Thickness	Direction of ankle rotation	Maximum deflection δ_m (mm)	Maximum medial–lateral displacement δ_z (mm)	Rotation angle θ_f (degrees)	Maximum von Mises stress σ_e (MPa)
Uniform	Plantar flexion	8.3	−3.9	3.0	16.2
	Dorsiflexion	6.7	2.3	2.6	15.1
Variable	Plantar flexion	8.9	−3.3	3.3	16.2
	Dorsiflexion	7.3	2.8	2.8	15.1

thickness variation may have a significant effect on analytical results, ideally therefore, it should be incorporated in the FEM model in order to achieve an accurate assessment of AFO stiffness. As anticipated, maximum stresses are not significantly affected by the adoption of a variable thickness model. Stress development can however be more evenly spread and a lighter AFO design achieved by a rational choice of thickness distribution.

4 VALIDATION

4.1 Description of tests by Sumiya *et al.*

The finite element model was validated by comparing its predictions with experimental data reported by other workers [**7**, **8**] investigating how the stiffness changes with ankle trimline variation. The reported data had been obtained by an experimental rig consisting of a moulded plaster artificial foot, which was attached to a metal pipe representing the tibia with a hinged joint positioned at the ankle axis. The pipe formed a sliding joint through the centre of a moulded plaster artificial calf. The AFO was secured to the calf by a strap and the posterior foot region was bolted to the underside of the plaster foot. A tensiometer was attached at some distance along, and perpendicular to, a metal bar, which was hinged at the ankle joint to act as a lever arm. The ankle moment applied to the bar in this manner was transferred to the AFO by a pin connecting the bar to the artificial foot; a protractor was centred at the ankle axis to measure the ankle angle. To apply a set deflection, the tensiometer was manually pulled at a slow angular velocity to approximate static loading conditions. The ankle axis was assumed to be at lateral malleolus height, perpendicular to the midline of the foot at its intersection with the anatomical ankle axis. After setting up each AFO in the testing device, the artificial foot was dorsiflexed and plantar flexed 15° at intervals of 2.5° and the ankle moment was calculated.

4.2 Modelling

Sumiya *et al.* (personal communication) provided additional data on mean measurements of the geometry of the 30 AFOs tested. In the absence of precise information about a specific specimen, the finite element model used was a modified version of the computer-generated one described earlier, duplicating as much as possible the shape of the trimline shown in Fig. 6 and having the mean dimensions of the specimens listed in Table 4. It was found that it was necessary to change the geometry of the shell of the leg used previously so that the medial–lateral width of the new model matched more closely that of the specimens tested. Also, the arch of the foot in the sagittal plane was straightened and the distal part of the foot region was made flatter. The thickness was initially assumed constant and equal to 3 mm to match the reported thickness of the polypropylene

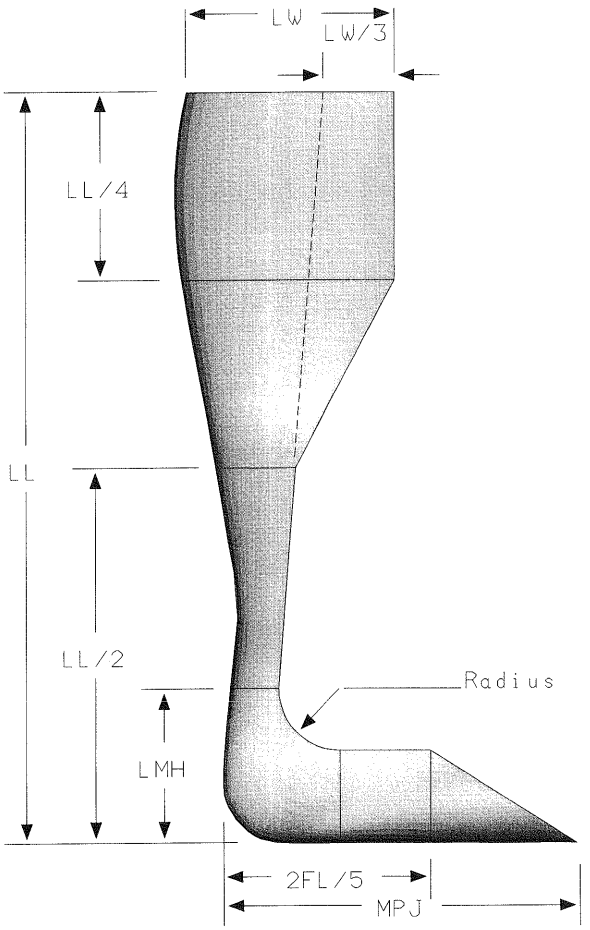

Fig. 6 Trimline of AFO specimens tested by Sumiya *et al.* [**7**, **8**] (LMH, lateral malleolus height; MPJ, metatarsophalangeal joint)

Table 4 Mean dimensions of specimens tested by Sumiya *et al.* (personal communication)

Specimen	Geometric parameter	Dimension (mm)
Leg	Length (LL)	350
	Maximum width (LW)	97.5
	Minimum width	67
	Height at minimum width	132.3
Malleoli	Lateral height	72.1
	Medial height	79.3
	Inter-malleolar distance	79.6
	Lateral distance from heel	50
	Medial distance from heel	59.7
Foot	Length (FL)	244.3
	1st MPJ* distance from heel	172.2
	5th MPJ distance from heel	159.8
	Maximum width	92.3

* MPJ = metatarsophalangeal joint.

sheet. Eventually, however, a thickness distribution was specified over the new model based, as with the previous model, on the measured thickness variation of a custom-made AFO. This change contributed significantly to the accuracy of the results. The ratio of the trimiline arc radius at the ankle to the lateral malleolus height (radius/LMH) was defined as the trimline shape parameter. The accuracy of the new FEM model was initially checked with radius/LMH = 0.4, which is equivalent to the '40 per cent trimline stage', according to the terminology of the reported experiment.

In order to simulate the action of the artificial leg on the calf region of the AFO, a subset of nodes, located posteriorly and anteriorly at the same level as the calf strap, were constrained radially so that the calf section was allowed to both rotate about and slide up or down the Y axis. Nodal constraints and displacements in the foot and heel regions were specified relative to a cylindrical coordinate system whose z axis coincided with the assumed ankle joint axis.

Displacement consistent with rigid body rotation of the foot about the ankle joint was applied to a number of nodes over the distal foot areas as shown in Fig. 7. This number was smaller for dorsiflexion than for plantar flexion because, as reported, during the experiment the dorsiflexion moment was applied via a pin over a small distal foot area while, for the plantar flexion, the plaster foot forced the whole foot region. The x and y directions of the nodal coordinate system, which coincided with the global radial and circumferential directions respectively, were rotated by an additional amount equal to the angle of imposed rotation so that this rotation could be produced exactly by the displacement imposed in the rotated y direction. This is illustrated in Fig. 7 which also shows that the imposed displacement on node i should be $R_i \sin\theta$ where R_i is the distance of node i from the ankle joint and θ is the angle of rotation.

Another set of nodes in the posterior foot region, lying near to or on the XY plane, was displaced both radially and circumferentially with respect to the same cylindrical coordinate system in a manner compatible with the finite rotation applied to the specimen in that region. As shown in Fig. 7, these two imposed displacements are equal to $R_i'(1-\cos\theta)$ and $R_i' \sin\theta$ respectively. Some of these nodes were also constrained in the z direction to simulate the local effect of bolting. The total ankle moment was calculated from the following equation,

$$M = \sum_{i(\text{foot})} F_{yi}(R_i \cos\theta + \delta_{xi}) + \sum_{i(\text{heel})} (F_{yi}R_i' \cos\theta - F_{xi}R_i' \sin\theta)$$

where F_{xi} and F_{yi} are the reactions at node i, and δ_{xi} and δ_{yi} are the corresponding nodal displacements.

4.3 Results for 5° rotation

The analytical and experimental results for the resisting moment about the ankle during dorsiflexions and plan-

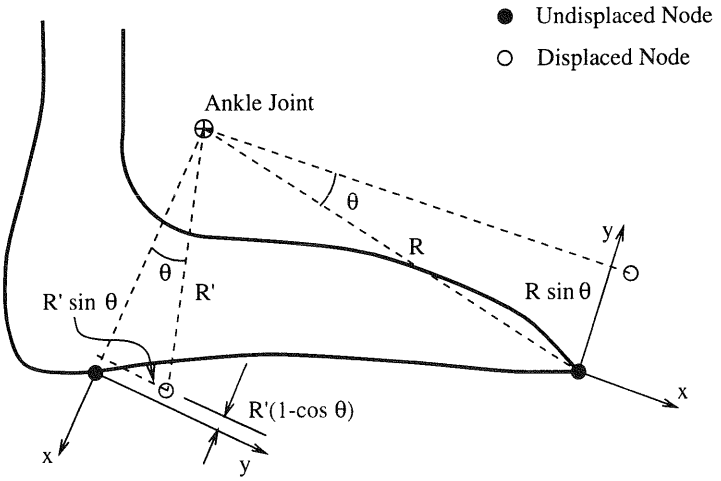

Fig. 7 Imposed displacements relative to nodal coordinate systems

tar flexions of 5° are plotted versus the corresponding trimline stages, as shown in Fig. 8. As pointed out earlier, a trimline stage is defined as the trimline's arc radius at the ankle divided by the height of the lateral malleolus, expressed as a percentage. This means that the 20 per cent stage corresponds to the stiffest specimen and the 60 per cent stage corresponds to the most flexible specimen. The difference between the measured and predicted moments appears to be small in most cases. The exceptions are the plantar flexion moments measured from the most flexible AFOs (>45 per cent trimline stage), which appear to be significantly lower than those predicted. These moments are also smaller than the respective measured dorsiflexion moments. This observation raises the possibility of inaccurate measurement or error in the original plot since it contrasts with the behaviour of all other AFO specimens (<45 per cent trimline stage), which exhibit greater resistance to plantar flexion than to dorsiflexion. It was reported by Sumiya *et al.* [7] that, although reliable measurements could be obtained from their simple device, errors could arise from the manual application of forces and friction between the pipe and artificial leg. The effect of such errors may have been more pronounced at lower values of measured resisting moment.

Von Mises stress contours revealed stress concentrations at the ankle trimline, on both medial and lateral edges. Significant stresses were also evident in the regions of imposed displacement, at the foot and below the ankle joint. A slight medio-lateral bulging of the ankle trimlines was noted during dorsiflexion for analyses with a more anterior (smaller 'stage') trimline.

4.4 Results for 15° rotation

Considerable convergence problems were encountered in attempts to simulate 15° responses for the various trimline stages. Solutions in both plantar flexion and dorsiflexion were directly obtained only for the most compliant, 60 per cent trimline stage AFO. In this case, the predicted ankle moments were found to be within ±10 per cent of measured values. It was however observed that the predicted variation of ankle moment with rotation did not follow the expected pattern. This was corrected by applying the rotation in a number of predefined steps at the start of which the nodal coordinate system was rotated by the same angle increment resulting in a gradual change of the orientation of the imposed displacement. Using 30 load steps, the final ankle moments for the 60 per cent trimline stage were found to be approximately the same as those obtained using the original loading scheme. However, the new analysis produced the expected drop in stiffness with increasing rotation in dorsiflexion, whereas a slight increase in stiffness was noted in plantar flexion.

For a stiffer AFO model, the solution was interrupted at a lower angle of rotation (around 11°) because of lack of convergence within the specified tolerances. The problem was attributed to the irregular pattern of rather large reaction forces at the constrained nodes, which created a large imbalance at the beginning of each load step. Thus, a more accurate representation of the forces transmitted by the foot was sought. Contact elements could not be used because this would require modelling of the foot itself. An alternative method was used with elastic spring elements representing the foot and connected to

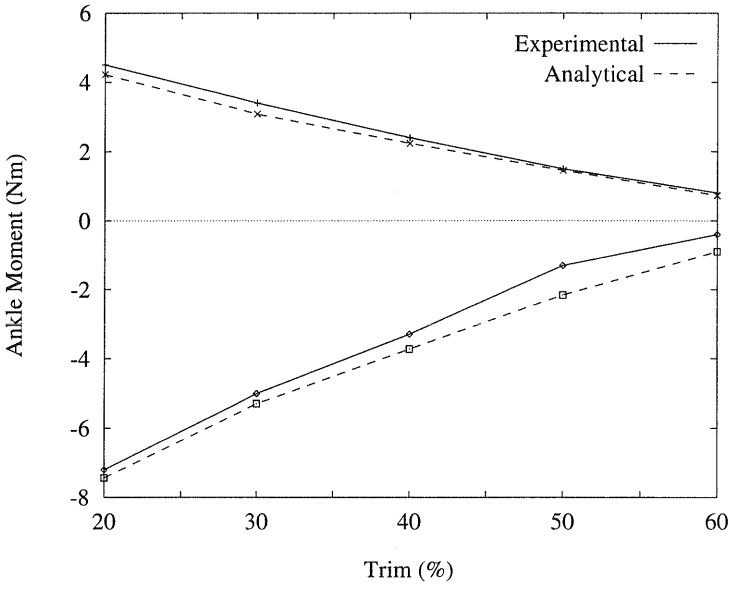

Fig. 8 Measured [8] and predicted ankle moment versus trimline stage for 5° rotation (dorsiflexion moments shown positive, plantar flexion moments shown negative)

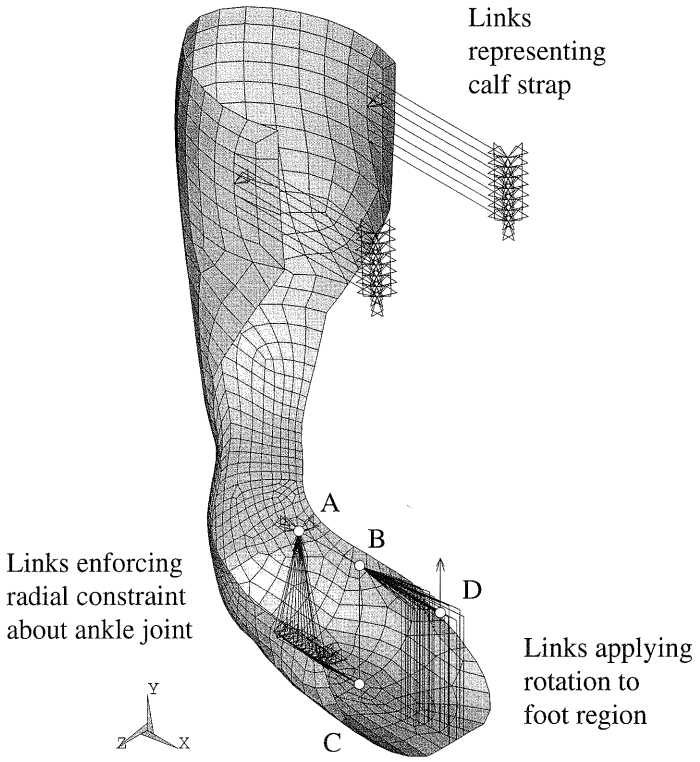

Fig. 9 Beam and spring elements representing the dorsiflexion action of the testing rig on the AFO

the nodes to be displaced. This method would yield acceptable results provided that the stiffness of the spring elements was adjusted so that it would model, to a certain extent, the interaction between the AFO and the limb. Various arrangements of spring elements were tried leading to the one shown in Fig. 9, which was selected as the most appropriate.

As shown in Fig. 9, constraints and displacements were imposed on nodes through a rigidly connected frame consisting of a horizontal beam element AB, a set of horizontal beam elements, such as BD, radiating out from B, and a vertical beam element BC. Spring elements connected the nodes below the ankle joint axis to point A lying at the intersection of this axis and the global XY plane (the mid-sagittal plane of the leg). Only the translational degrees of freedom were constrained at A allowing free rotation of the frame about the ankle joint axis. Displacement was imposed to the nodes below the ankle axis through springs connecting them to point C of the frame. Finally, displacement was imposed to the nodes in the foot region through spring elements, parallel to the global Y direction, connecting them to end points of the horizontal beams radiating from B.

The analysis was applied to the AFO model with a 40 per cent trimline stage and spring stiffness of 1000 N/mm, which was estimated to produce a maximum spring extension of 0.1 mm. Although the final rotation angle of 15° was again not achieved, intermediate ankle moment results at 5° rotation showed better agreement with the reported experimental data than those predicted by imposing displacements directly on the nodes. Due to time and hardware limitations, it was decided to pursue a 15° solution with a more compliant model. Using a link stiffness of only 1 N/mm, complete results were obtained for both dorsiflexion and plantar flexion; these are listed in Table 5.

Table 5 Predictions for the model with a 40 per cent trimline stage loaded through elastic springs

Direction of ankle rotation	Rotation angle θ_f (degrees)	Ankle moment M (N m)		Discrepancy (%)
		Numerical	Experimental	
Plantar flexion	5	2.2	3.3	−33
	15	7.3	13.3	−45
Dorsiflexion	5	1.7	2.4	−29
	15.7	3.6	5.5	−35

The table shows a considerable discrepancy between predicted and measured moments. This was expected since the assumed compliance of the links does not, in any way, represent that of the rigid plaster foot through which rotation was imposed in the tests. These results are however interesting since they show that a softer, more compliant foot material, as is the case with human tissue, can achieve larger rotations on an AFO with much less effort than that required using a relatively rigid artificial foot. The moment versus angle relationship for dorsiflexion shown in Fig. 10 becomes strongly non-linear at large angles approaching a limit load asso-

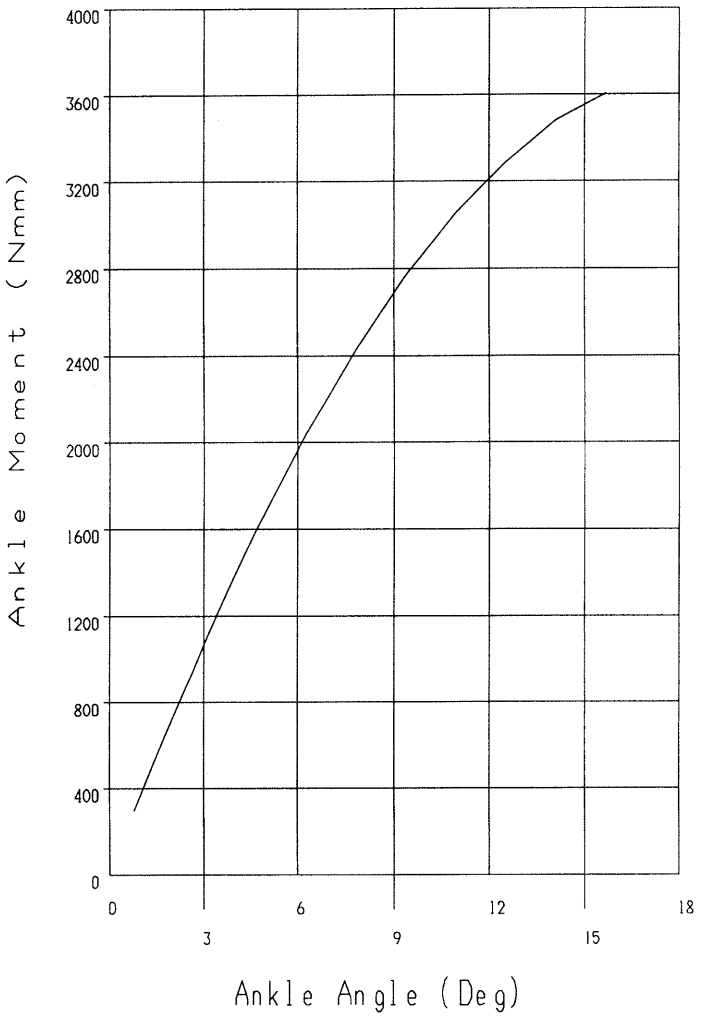

Fig. 10 Ankle moment versus angle of rotation for the 40 per cent trimline stage AFO in dorsiflexion imposed through elastic springs

ciated with catastrophic (snap) buckling according to the classical stability theory [**24**].

5 CONCLUSIONS

Once the patient's requirements have been assessed, the orthotist is faced with the selection of an AFO design with the ability to fulfil these requirements. The finite element method has been proposed as a means of predetermining desirable AFO characteristics directly, thus avoiding lengthy trial and error procedures. It is hoped that this approach would lead to better patient care at a much lower cost.

The key to the success of the application of the finite element method and, indeed, of any other predictive tool, is its effectiveness and its accuracy. Both these issues have been addressed in this paper. As several previous attempts have indicated, the problem is a complex one and it would take some time before a definitive strategy is adopted. In the FEM analyses by Leone *et al.* [**14**, **15**] for instance, the AFO model was free from any heel constraint and the stiffness (or flexibility) was identified from the predicted load–deflexion relation. This relation is, however, position dependent in contrast to the more objective moment–angle relation used by several experimenters [**2**, **5**, **7**, **8**] as well as in the present work. The linear analysis by Leone *et al.* [**14**] produced a constant flexibility value for every location where the foot deflexion was predicted. Their non-linear analysis [**15**] produced a load-dependent flexibility but, as pointed out in the Introduction, their numerical results deviated considerably from their own test data. Other reported linear FEM analyses relied on coupled AFO–foot models and focused on either the stiffening effect of the AFO on the foot [**12**, **13**] or the level of stresses developing in the AFO [**16**]. The results of such analyses are not therefore relevant or comparable with those presented in this paper.

Certain important questions have been posed in this work which has been basically concerned with the prediction of the stiffness of a plastic AFO in the sagittal

plane, i.e. its response to plantar flexion and dorsiflexion movements of the foot. The central argument has been that the device is highly likely to undergo excessive deformation during which its material cannot remain linearly elastic. The finite element models developed were therefore based on the principles of geometric and material non-linearity. Preliminary applications of these models under moderate loading conditions indicated significant differences between predictions of linear and non-linear behaviour. This provided an initial justification for the more advanced analysis.

The critical tests for accuracy and effectiveness then followed. Reliability was assessed through simulations of experiments in which AFO specimens of variable geometry were subjected to considerable deformation. In general, analytical predictions were found to be in good agreement with test measurements. One important practical consequence, borne out by experimental evidence, is that the stiffness of a dorsiflexed AFO drops at high rotations while that of a plantar flexed AFO increases slightly. Regarding the effectiveness of the simulations, two very influential factors were identified: the accuracy of geometric representation and the limitations of the available software.

The gradual process of achieving a model that would increasingly reflect the testing environment, as reported by its designers, showed that a superficial resemblance of geometric features is not sufficient for good agreement between analytical and experimental results. Adjusting the width and the thickness of the AFO model to more realistic values as well as adopting a more accurate representation of the applied rotation were the more critical steps towards reliable predictions. It is worth noting that this was achieved without a full documentation of the experimental set-up and with the results available as averages from a number of similar specimens of slightly variable geometry.

The difficulties experienced in predicting large deformations were closely related to the stiffness of the model. The success of an iterative process, on which a non-linear analysis is based, depends on the maximum number of iterations allowed by the program as well as on the magnitude of the error tolerance adopted. An intelligent combination of these two parameters as well as optimum use of software and hardware resources may lead to predictions of very large deformations for very stiff models. It was shown however, that the more realistic the modelling of loading and support conditions, the easier it is for the FEM model to converge to non-linear AFO responses.

Since the developed analysis was three-dimensional, it produced medio-lateral displacements and rotations about axes other than the ankle joint axis. Such important results have not been quantified or discussed in detail because it was felt that they deserve particular attention, which is outside the scope of this paper. The interpretation, validation and practical implications of these predictions can be achieved by their correlation and comparison with results of experimental studies on coupled AFO motions [**10**].

The results presented are simply indicative of the FEM potential as an assessment and design tool prior to prescription. Through the developed procedure, an orthotist can obtain reliable information on the deformation-dependent stiffness characteristics of an initial AFO design. If these characteristics do not meet the patient's requirements, the modelling and analysis strategies adopted are sufficiently versatile to allow virtual modifications so that an optimum design could be achieved. Such an iterative process requires a high level of confidence in the FEM simulation. This can be established through additional validation programmes incorporating wider geometric variations in designs, modelling of the AFO–limb–shoe interaction, as well as dynamic/viscoelastic material behaviour.

ACKNOWLEDGEMENT

The authors would like to thank Dr Tadashi Sumiya of EIREC, Nagoya, Japan, for kindly providing them with additional detailed information on the AFO specimens used in his experiments.

REFERENCES

1 **Halar, E.** and **Cardenas, D. D.** Ankle-foot orthoses: clinical implications. *Phys. Med. Rehabil.*, 1987, **1**(1), 45–66.
2 **Condie, D. N.** and **Meadows, C. B.** Some biomechanical considerations in the design of ankle-foot orthoses. *Orthotics and Prosthetics*, 1977, **31**(3), 45–52.
3 **Lehmann, J. F., Esselman, P. C., Ko, M. J., Smith, J. C., Delateur, B. J.** and **Dralle, A. J.** Plastic ankle-foot orthoses: evaluation of function. *Arch. Phys. Med. Rehabil.*, 1983, **64**, 402–407.
4 **Golay, W., Lunsford, T., Lunsford, B. R.** and **Greenfield, J.** The effect of malleolar prominence on polypropylene AFO rigidity and buckling. *J. Prosthetics Orthotics*, 1989, **1**(4), 231–241.
5 **Yamamoto, S., Ebina, M., Iwasaki, M., Kubo, S., Kawai, H.** and **Hayashi, T.** Comparative study of mechanical characteristics of plastic AFOs. *J. Prosthetics Orthotics*, 1993, **5**(2), 59–64.
6 **Lunsford, T. R., Ramm, T.** and **Miller, J. A.** Viscoelastic properties of plastic pediatric AFOs. *J. Prosthetics Orthotics*, 1994, **6**(1), 3–9.
7 **Sumiya, T., Suzuki, Y.** and **Kasahara, T.** Stiffness control in posterior-type plastic ankle-foot orthoses: effect of ankle trimline, Part 1: a device for measuring ankle moment. *Prosthetics Orthotics Int.*, 1996, **20**(2), 129–131.
8 **Sumiya, T., Suzuki, Y.** and **Kasahara, T.** Stiffness control in posterior-type plastic ankle-foot orthoses: effect of ankle trimline, Part 2: orthosis characteristics and orthosis/patient matching. *Prosthetics Orthotics Int.*, 1996, **20**(2), 132–137.

9 **Nagaya, M.** Shoehorn-type ankle-foot orthoses: prediction of flexibility. *Arch. Phys. Med. Rehabil.*, 1997, **78**, 82–84.

10 **Klasson, B., Convery, P.** and **Raschke, S.** Test apparatus for the measurement of the flexibility of ankle-foot orthoses in planes other than the loaded plane. *Prosthetics Orthotics Int.*, 1998, **22**(1), 45–53.

11 **Lord, M.** and **Jones, D.** Issues and themes in computer aided design for external prosthetics and orthotics. *J. Biomed. Engng*, 1988, **10**, 491–498.

12 **Lam, P. C., Reddy, N. P.** and **Downing, M.** Effects of heel and toe forces on ankle-foot orthoses design using finite element analysis. *ASME Des. Engng Div. (Publ.)*, 1986, **1**, 49–52.

13 **Lam, P. C., Reddy, N. P.** and **Downing, M.** Dynamic responses of ankle-foot orthoses. *ASME Bioengng Div. (Publ.)*, 1986, **2**, 130–131.

14 **Leone, D., Diemente, S., Gustave, S.** and **Lopez-Isa, M.** Structural analysis of solid ankle-foot orthoses. Proceedings of the 14th Annual Northeast Bioengineering Conference, Durham, New Hampshire, 1988, pp. 26–28.

15 **Leone, D., Diemente, S.** and **Lopez-Isa, M.** Structural stability prediction for thermoplastic ankle-foot orthoses. In Proceedings of the 17th Annual Northeast Bioengineering Conference, Hartford, Connecticut, April 1991, pp. 231–232.

16 **Chu, T. M., Reddy, N. P.** and **Padovan, J.** Three-dimensional finite element stress analysis of the polypropylene, ankle-foot orthosis: static analysis. *Med. Engng Physics*, 1995, **17**(5), 372–379.

17 *ANSYS User's Manual for Revision 5.1*, Vols I–IV, 1994 (Swanson Analysis Systems Inc., Houston).

18 **Arnold, M. A.** Finite element analysis of ankle foot orthoses. PhD thesis, Department of Mechanical Engineering, University of Southampton, 1999.

19 **Callister, W. D.** *Materials Science and Engineering: An Introduction*, 2nd edition, 1991 (John Wiley and Sons, Chichester).

20 **Williams, J. G.** *Stress Analysis of Polymers*, 1973 (Longman, London).

21 **Ogorkiewicz, R. M.** *Engineering Design Guides 17—The Engineering Properties of Plastics*, 1977 (Oxford University Press, Oxford).

22 *Data Sheets on the Physical, Mechanical and Thermal Properties of Various Polymers*, Issue 1, 1995 (North Sea Plastics Limited, Glasgow).

23 **Birley, A. W.** and **Scott, M. J.** *Plastic Materials: Properties and Applications*, 1982 (Leonard Hill, Glasgow).

24 **Thompson, J. M. T** and **Hunt, G. W.** *A General Theory of Elastic Stability*, 1973 (John Wiley, London).